Adhesion of melanoma cells to the microsphere surface is reduced by exposure to nanoparticles

Hiroyuki Shinto,* Yoshinori Ohta, and Tomonori Fukasawa

Department of Chemical Engineering, Kyoto University, Katsura Campus, Nishikyo-ku, Kyoto 615-8510, Japan

Phone: +81-75-383-2671, Fax: +81-75-383-2651, e-mail: shinto@cheme.kyoto-u.ac.jp

Abstract

It is of fundamental importance to better understand the interactions of nanoparticles with mammalian cells, such as cellular uptake of nanoparticles and the resultant cellular responses. In the present study, we have measured the interaction force of single nanoparticle-treated cells with a microsphere surface, using atomic force microscopy (AFM) with colloid probes. It was found that the adhesion force of murine melanoma cells to the surface of a 6.90-µm carboxyl-modified polystyrene (PS-COOH) microsphere was significantly reduced by exposing them to the 40-nm PS-COOH nanoparticles in a serum-free culture medium for 15 min, although the nanoparticle treatment of the cells up to 180 min hardly affected their morphology, membrane integrity, and metabolic activity. Possible mechanism of this phenomenon will be discussed.

Graphical Abstract
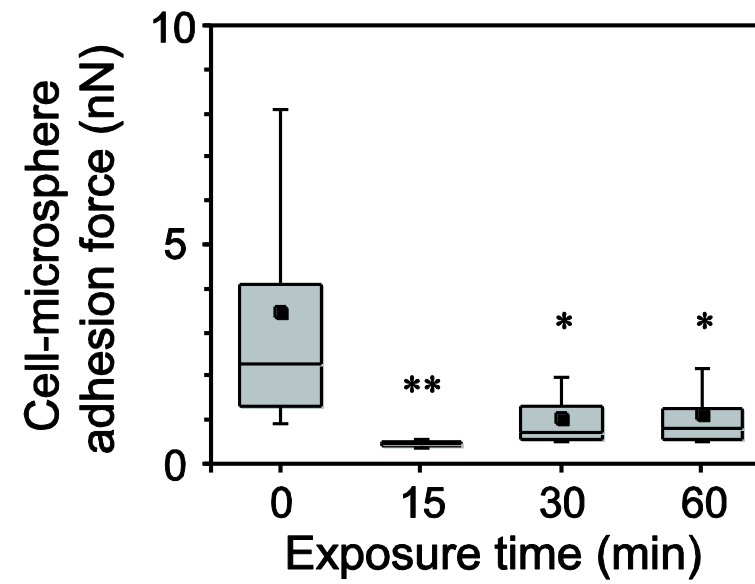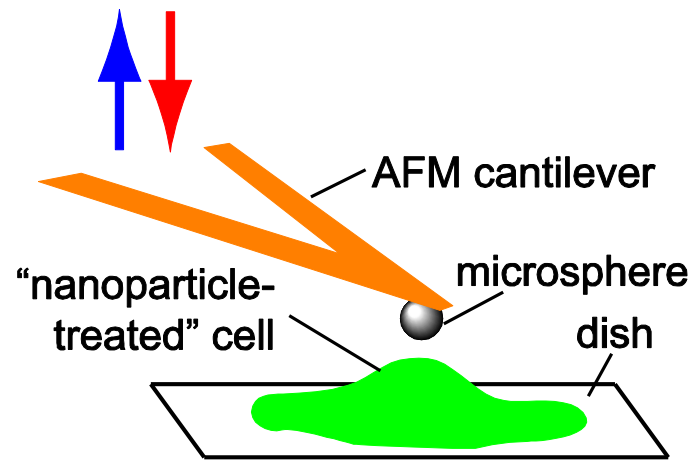
1. Introduction

In the past decade, nanoparticles and their interactions with the soft surfaces of biological systems like cells have been a focus of many research groups [1]. This is largely because many kinds of manufactured nanoparticles have promising application in the field of biomedicine such as biosensors, drug delivery, gene delivery, and disease diagnoses/therapy, where the interactions of nanoparticles with cells play key roles in performing their biomedical functions [2]. On the other side of this, one of the major concerns regarding applications of the nanoparticles is the potential risks such as toxic effects adverse to human health due to their small size, high reactivity, and large surface area [2-5]. The widely studied and used nanoparticles include metals [2,5,6], metal oxides [5-7], silica [8,9], carbon-based nanoparticles [2,5,6], polymeric nanoparticles [1,10], and quantum dots [2,5]. Cellular uptake, location and translocation, and resultant cytotoxicity of these nanoparticles have been extensively investigated and published in lots of literatures (see the references cited in Refs. [1-10]). No literature has reported on how the adhesion of mammalian cells to substrata is affected by nanoparticle treatment, although this cell−substrate adhesion plays a fundamental role in many processes within multicellular organisms. These processes include the formation and the cohesion of tissues, cell differentiation, cell motility, and pathologies such as cancer proliferation and metastasis.

In our previous study [11], we have measured the interaction forces of the murine melanoma cells with the single polystyrene (PS) microspheres of different surface chemistries in serum-free culture media. The results indicate that the unmodified hydrophobic polystyrene (unmodified PS) microspheres interact weakly with the cell surfaces through van der Waals forces and hydrophobic forces, whereas the carboxyl-modified polystyrene (PS-COOH) microspheres interact rather strongly with the cell surfaces via integrins that are transmembrane adhesion molecules acting as cell-adhesion receptors. Likewise, the PS-COOH nanoparticles, rather than the unmodified PS nanoparticles, are expected to have great impact on the adhesion of cells to substrata. The aim of the present study is to demonstrate how the adhesion of mammalian cells to substrata is affected by nanoparticle treatment.

In the present study, we report for the first time the adhesion of "nanoparticle-treated cells" to a substrate using atomic force microscopy with colloid probes, which enabled us to measure the interaction forces between a living cell and a microsphere in a culture medium [12]. We employed the murine melanoma cells as the target cells, the fluorescent PS-COOH nanoparticles as those incubated with the cells in a culture medium, and the PS-COOH microspheres as the substrate for cell adhesion. Cellular uptake of the nanoparticles as well as morphology, membrane integrity, and metabolic activity of the nanoparticle-treated cells were also investigated.

2. Materials and methods

2.1. Cell line and culture conditions

The murine melanoma cell line (B16F10; kindly provided by Profs. Fukumori and Ichikawa of Kobe Gakuin University, Kobe, Japan) was cultured in a complete medium composed of an MEM medium (05900, Eagle's minimum essential medium with kanamycin, without L-glutamine or sodium bicarbonate; Nissui Pharmaceutical, Tokyo, Japan), L-glutamine (16919-42; Nacalai Tesque, Kyoto, Japan) and 10% fetal bovine serum (FBS; JRH Biosciences, Lenexa, KS, USA); additionally, sodium bicarbonate (31213-15; Nacalai Tesque) was used to adjust the pH to 7.4. In prior to use, the FBS was heat-inactivated. The cells were stationarily cultivated in a 75-cm^2 flask (3110-075; IWAKI, Tokyo, Japan) containing a 10-mL complete medium, and the flask was stored in an incubator, inside which a moist atmosphere of 5.0% CO_2 was maintained at temperature of 37.0 °C. The complete medium was changed every 2 days. The cells were subcultured every 4 days, when they formed a subconfluent monolayer of the surface density 0.7×10^5 cells/cm^2. All water used in the experiments was purified using an Autopure system (WD500; Yamato Scientific, Tokyo, Japan) to give a resistance of 18.2 MΩ cm and a total organic carbon of less than 50 ppb.

2.2. Nanoparticles

The green-fluorescent polystyrene (PS) nanoparticles of carboxyl-modified surfaces, referred to as PS-COOH nanoparticles in the present study, were purchased from micromod Partikeltechnologie (Rostock Warnemünde, Germany). The PS-COOH nanoparticle suspension was diluted with Dulbecco's modified Eagle medium (DMEM, 21063-029; GIBCO, Grand Island, NY, USA), which contained 4500 mg/L D-glucose, L-glutamine, and 25 mM HEPES buffer but no sodium pyruvate or phenol red. The culture media including the nanoparticles were prepared at desired concentrations and kept in clean sterile vessels. These nanoparticle-containing media were stocked in the refrigerator and used within a week after the preparation. The media including nanoparticles were warmed up at 37.0 °C and sonicated for 5 min just prior to use for exposure of the cells to the nanoparticles. Here, FBS was never added for eliminating the effects of serum proteins on the experimental results. The nanoparticles suspended in water and DMEM were characterized with respect of hydrodynamic diameters and zeta potentials, using Zetasizer Nano ZS (Malvern Instruments, Worcestershire, UK).

2.3. Exposure of cells to nanoparticles

The cells were seeded in different containers for different purposes: (i) a ϕ35-mm dish with ϕ27-mm glass bottom (3910-035; IWAKI) for CLSM and AFM; (ii) 9-mm × 9-mm coverslips (Matsunami, Osaka, Japan) being sank into a 24-well plate (3820-024; IWAKI) for SEM; (iii) a 25-cm^2 flask (3102-025; IWAKI) for trypan blue assay; (iv) a 96-well plate (3860-096; IWAKI) for LDH and ATP assays. Before use, the coverslips were sterilized in ethanol overnight, washed thoroughly in water, and dried in air inside a bio-clean bench. For these subcultures in containers (i)–(iv), the 75-cm^2 flask with the subconfluent monolayer cells prepared as explained in Section 2.1 was first rinsed with 10 mL of Dulbecco's phosphate-buffered saline without calcium or magnesium (DPBS, 21600; GIBCO) after

removal of the complete medium (FBS-supplemented MEM); subsequently, the cells were separated from the base of the flask by trypsinization with a 1-mL DPBS solution of 0.25% trypsin and 0.02% EDTA. A fresh 9-mL complete medium was then added into the 75-cm^2 flask, giving a 10-mL cell suspension of $5{\times}10^5$ cells/mL. Proper amounts of this cell suspension and the complete medium were filled in fresh containers (i)–(iv) to satisfy the desired cell concentrations: $0.2{\times}10^5$ cells/cm^2 for CLSM, SEM, and trypan blue assay; $0.4{\times}10^5$ cells/cm^2 for LDH and ATP assays; $1.0{\times}10^5$ cells/cm^2 for AFM. For stationary cultivation, 0.25 mL of the cell suspension was added into a fresh 75-cm^2 flask including a fresh 10-mL complete medium, giving a cell concentration of $2{\times}10^3$ cells/cm^2.

After 1-day incubation, the cell samples were rinsed with DPBS after removal of the complete medium and filled with the DMEM solutions of different nanoparticle concentrations of $C_p = 0$, 0.01, 0.02, 0.04, and 0.08% v/v, which were prepared as in Section 2.2. These samples were stored in the incubator for desired exposure periods ($t_{exp} = 0$, 15, 30, 60, 90 and 180 min), and then employed for different purposes as will be explained below.

2.4. Confocal laser scanning microscopy (CLSM)

The nanoparticle-containing media were removed from the cell samples in the glass-bottom dishes prepared as in Section 2.3, and the cells therein were rinsed twice with DPBS. 2.5 mL of fresh DMEM without nanoparticles or FBS was filled in the dish. The differential interference contrast (DIC) and the fluorescence images of the cell samples were obtained by CLSM (C1si-ready mounted on TE2000-E; Nikon, Tokyo, Japan) with the water-immersion objective 60× of N.A. = 1.20 (VC60×WI; Nikon) and the air-cooled ion laser of 488-nm wavelength (163-C1207; Spectra-Physics, Irvine, CA, USA). A z-series of the optical sections of 0.45-µm thickness ($=\Delta z$) was acquired from the bottom surface of $z = 0$ to the media region of $z = 19.8$ µm ($=N_z\,\Delta z$; $N_z = 44$), which sufficiently covered the individual cells with a height of about 5 µm. A z-series of the fluorescence images was analyzed using the built-in software (EZ-C1; Nikon) to give the fluorescence per cell:

$$\text{Fluorescence per cell} = \left\langle \bullet_{k=0}^{N_z} \left[FL_i(k) - FL_i(N_z) \right] \right\rangle_i \tag{1}$$

where $FL_i(k)$ denotes the fluorescence of i-th cell at k-th optical section with the xy-area of the basal cellular region, and the brackets $\langle L \rangle_i$ denote the cell-averaged quantity of the function enclosed therein. It is noted that $FL_i(k)$ for sufficiently large k (>15) gives the background. The value of Eq. (1) gives the uptake amount of the nanoparticles onto/into a cell. Every sample was measured in sextuplicate.

2.5. Scanning electron microscopy (SEM)

The cell samples on the coverslips prepared as in Section 2.3 were rinsed with DPBS after removal of the nanoparticle-containing media. The samples were fixed with paraformaldehyde, post-fixed with OsO_4, and dehydrated in an ethanol series and t-butyl alcohol, followed by being frozen in a small amount of t-butyl alcohol and freeze-dried, as described elsewhere [11]. Finally, the samples were sputtered with a conductive layer of 5-nm thickness gold using an Emitech K575XD (Quorum Technologies, Ashford, UK) and imaged using a Keyence VE-8800 (Osaka, Japan).

2.6. Trypan blue dye exclusion assay

The cell samples in 25-cm^2 flasks prepared as in Section 2.3 were washed twice with DPBS after removal of the nanoparticle-containing media. The cells were separated from the substrate by trypsination with a 0.4-mL DPBS solution of 0.25% trypsin and 0.02% EDTA, and then a 3.0-mL complete medium was added. Equal amounts (20.0 µL) of this cell suspension and a 0.5% trypan blue stain solution (29853-34; Nacalai Tesque) were mixed together in a microtube. After applying this mixture into a TC10 counting slide, we counted the dyed and undyed cells using a TC10 automated cell counter (Bio-Rad Laboratories, USA) to estimate the cell viability:

$$\% \text{ dye exclusion} = \frac{(\text{Number of undyed cells})}{(\text{Number of dyed cells}) + (\text{Number of undyed cells})} \pm 100 \qquad (2)$$

Every sample was measured in triplicate.

2.7. LDH and ATP assays

LDH (lactate dehydrogenase) and ATP (adenosine triphosphate) assays were done using the CytoTox-ONE homogeneous membrane integrity assay and the CellTiter-Glo luminescent cell viability assay (Promega Corporation, Madison, WI, USA), respectively. The 96-well plate prepared as in Section 2.3 had not only a nanoparticle-containing culture medium of 200 µL with adherent cells in each well, but a culture medium with cells (for the maximum LDH release control and the maximum ATP content control) and a medium without nanoparticles or cells (for the background control). After incubation for desired exposure periods, 10 µL of lysis solution (a 2.7% (w/v) solution of Triton X-100 in water) was added to the wells for the maximum LDH release control. The 96-well plate was then centrifuged at a gravitational field of 100 g for 3 min so that the dead cells suspended in the medium should have settled down.

For LDH assay, 100 µL of the supernatant in each well was transferred to a 96-well black plate with non-binding surface (3650; CORNING, Corning, NY, USA). After being treated according to the manufacturer's instructions, the samples in individual wells were monitored by an automated plate reader (Infinite M200; Tecan, Grödig, Austria) with an excitation wavelength of 560 nm and an emission wavelength of 590 nm. Cytotoxicity was calculated by the formula:

$$\% \text{ LDH release} = \frac{(\text{LDH release from treated cells}) - (\text{Culture medium background})}{(\text{Maximum LDH release}) - (\text{Culture medium background})} \pm 100 \qquad (3)$$

For ATP assay, the 96-well plate with the remained contents of 100 µL was equilibrated at 22.0 °C for 30 min and 100 µL of the CellTiter-Glo reagent was then added to each well. After being treated according to the manufacturer's instructions, 175 µL of the mixture in each well was transferred to a 96-

well white plate (3620-096; IWAKI), which was then allowed to incubate at 22.0 °C for 10 min to stabilize luminescent signal. The luminescence from the samples in individual wells were recorded by Infinite M200 with an integration time of 1 s per well. Cell viability was calculated by the formula:

$$\% \text{ ATP content} = \frac{(\text{ATP content inside treated cells}) - (\text{Culture medium background})}{(\text{Maximum ATP content}) - (\text{Culture medium background})} \times 100 \tag{4}$$

Every sample was measured in sextuplicate for LDH and ATP assays.

2.8. Atomic force microscopy (AFM) and colloid probes

Our methods for AFM measurements were explained elsewhere [11]. Briefly, an AFM probe (Model NP; Veeco Instruments, Santa Barbara, CA, USA), which has a V-shaped, 200-μm long cantilever with a spring constant of 0.06 N/m, was used. The carboxyl-modified PS microspheres of diameter 6.90 ± 0.41 μm were purchased from Bangs Laboratories (Fishers, IN, USA) and are hereafter referred to as PS-COOH microspheres. The zeta potentials of the PS-COOH microspheres in water and DMEM were measured using Zetasizer Nano ZS, as listed in Table 1. For preparation of colloid probes, a single microsphere was glued to the end of the cantilever. The cell samples in the glass-bottom dishes prepared as in Section 2.3 were washed twice with DPBS after removal of the nanoparticle-containing media. The dishes were filled with 2.5 mL of serum-free, nanoparticle-free, fresh DMEM (containing 25 mM HEPES buffer) so that the pH of the solution therein was maintained at 7.4 even in the outside environment for several hours. FBS was never added to the DMEM solution for AFM measurements, eliminating the effects of serum proteins on the experimental results.

An MFP-3D-SA AFM (Asylum Research, Santa Barbara, CA, USA) was used to measure the interaction forces between a living cell and a colloid probe in the DMEM solution at room temperature (25 ± 2 °C). The colloid probe was positioned over the nucleus of a living cell and the force measurement was then started within 5 min after the preparation of the cell samples. In measurement of a compression force curve, the colloid probe was brought in contact with the cell at a speed of 1.0 μm/s,

and a minimum indentation depth of about 1 µm required for the probe to reach the cell surface and to give a compliance region. This Z-scan speed was confirmed to be low enough to reduce or eliminate the hydrodynamic effects in the compression/decompression force curves. Once the indentation depth reached the typical values of 1.3 ± 0.5 µm, resulting in the loading (or pushing) forces of 0.4 ± 0.2 nN, the colloid probe was then allowed to reside on the cell surface for 5 min, during which time the cell did not migrate but deformed due to the contact with the probe. After this predefined dwell time of 5 min, the probe was moved away from the cell surface. In the case of strong adhesions between the cell and the probe, they did not always separate completely after the force cycle of compression, residence, and decompression. For this reason, the probe was moved to another place after the force cycle, and then immediately returned to its original position, in order to break any remaining bonds between the probe and cell; thereafter, another compression force curve was then collected, the baseline of which was used to define the zero force position for the decompression force curve. Another force measurement was carried out using a fresh cell sample in the same way as mentioned above. Thus, every force measurement was accomplished within about 10 min after the preparation of a cell sample. By repeating this procedure, 8−10 force curves were obtained for four types of the cell samples: $t_{exp} = 0$, 15, 30, and 60 min at $C_p = 0.08\%$ v/v.

2.9. Data analysis

The collected data of the CLSM fluorescence and the trypan blue/LDH/ATP assays were expressed as the mean $\pm$ standard error of mean (s.e.m.). The force–displacement curves obtained from AFM were analyzed using IGOR Pro software, with which the MFP-3D-SA AFM system was equipped. Steel's test was carried out for multiple comparison of the treated groups with the control group, using Microsoft Excel 2003 software with its add-in of Ekuseru-Toukei 2010 (Social Survey Research Information, Tokyo, Japan). $P \leq 0.05$ was considered statistically significant.

3. Results and discussion

3.1. Characterization of PS-COOH nanoparticles

As listed in Table 1, the PS-COOH nanoparticles in water exhibited the Z-average size of 40.0 nm with the relatively small PDI of 0.12 and the significantly large zeta potential of −34 mV in magnitude. The Z-average size and PDI of the PS-COOH nanoparticles in DMEM were almost the same as those in water, although the nanoparticles had the zeta potential of −11 mV in DMEM, which was significantly smaller in magnitude than that in water. These results suggest that the PS-COOH nanoparticles stably dispersed not only in water, but in DMEM of a high ionic strength (>140 mM).

3.2. Cellular uptake of nanoparticles and cell morphologies

Using CLSM, the B16F10 cells were observed after being exposed to the 40-nm PS-COOH particles at $C_p = 0.08\%$ v/v for different exposure periods. Typical CLSM images are displayed in Fig. 1a and b, showing that the cell took up the nanoparticles. The z-series of the optical sections indicates that the internalized nanoparticles were distributed throughout the cells and also accumulated in the perinuclear region of the cells. The results are comparable to those of the earlier study by Rejman et al. [13], where the B16F10 cells were incubated in a serum-free medium including 50-nm unmodified PS particles.

As in Fig. 1c, the cellular uptake amount of the nanoparticles significantly increased with t_{exp} for the first tens of minutes, while the uptake rate gradually slowed down. The uptake amount reached to a plateau within $t_{exp} = 60$ min. Following Guarnieri et al. [14], we could hypothesize that at earlier time the nanoparticles immediately absorb onto cell membrane and only later they enter the cells. Even though the mechanisms of this cellular entry by synthetic nanoparticles are still under debate, the best-described mechanism is endocytosis, referring to an energy-dependent uptake process in which the

11

nanoparticles are engulfed in pinched-off vesicles (i.e. endosomes) that carry the ingested nanoparticles into the cellular interior [15]. In addition, some nanoparticles may slip directly through the surface membrane of mammalian cells, similar to processes observed in bacteria [16]. Because the endocytosis is governed by a saturation-like kinetics [14], our data of uptake kinetics were also fitted by a saturation rate equation:

$$FL = FL_\infty \frac{t_{exp}}{t_{half} + t_{exp}} \tag{5}$$

where FL is the fluorescence per cell, FL_∞ the value of FL at equilibrium, and t_{half} the uptake half life. We obtained $t_{half} = 21.6$ min, which is comparable to $t_{half} = 4.7$ min for the earlier study of Guarnieri et al. [14], where the porcine aortic endothelial cells were incubated in a serum-free medium including 44-nm unmodified PS particles at a relatively high concentration of $C_p = 0.5\%$ v/v. Within the exposure periods up to $t_{exp} = 180$ min, there were no significant differences in the CLSM images between the treated cells and the intact untreated cells.

SEM was used to illustrate the apical surface of the B16F10 cells and the typical micrograph is shown in Fig. 2. The apical surface of the cells appeared to be rather rough and exhibited microvilli and microridges. Although a number of PS-COOH nanoparticles would attached to the outer surface of cells, they were too small (about 40 nm) to be individually identified by SEM. There were no significant differences between the treated and the untreated cells within the exposure periods up to $t_{exp} = 180$ min, as in the case with the CLSM. These results indicate that the morphologies of the B16F10 cells were hardly affected by the exposure to the 40-nm PS-COOH particles under our experimental conditions.

3.3. Membrane integrity and metabolic activity of nanoparticle-treated cells

The percentages of dye exclusion, LDH release, and ATP content are shown in Fig. 3a, b, and c, respectively, as a function of the particle concentration C_p for $t_{exp} = 30$ and 180 min: The former two quantities are associated with the membrane integrity of cells, and the latter is related to the metabolic

activity of cells. The percentages of dye exclusion remained very large and exceeded 96% even after the particle exposures of $C_p = 0.01–0.08\%$ v/v and $t_{exp} = 30–180$ min, which were almost the same as the dye-exclusion percentage in the case of no particle exposure ($C_p = 0$). The percentages of LDH release remained very small and were almost the same as that in the case of no particle exposure ($C_p = 0$). The percentages of ATP content remained fairly constant even after the particle exposure. These results indicate that both the membrane integrity and the metabolic activity of the B16F10 cells were hardly affected by the exposure to the 40-nm PS-COOH particles up to the concentration of $C_p = 0.08\%$ v/v and the period of $t_{exp} = 180$ min.

3.4. Force–displacement curves of a microsphere interacting with a nanoparticle-treated cell

The 180-min exposure of cells to the 40-nm PS-COOH particles up to the concentration of $C_p = 0.08\%$ v/v hardly affected the morphology, the membrane integrity, and the metabolic activity of the B16F10 cells, as mentioned in Sections 3.2 and 3.3. For further examination of the cellular responses to the PS-COOH nanoparticle exposure, we investigated the adhesion of the nanoparticle-treated cells onto the surface of the 6.90-µm PS-COOH microseres using colloid-probe AFM. Figure 4a shows a typical force–displacement curve during compression and decompression measured between the nanoparticle-treated cell and PS-COOH microsphere in serum-free, nanoparticle-free culture media. The compression curve displayed zero force at the distances longer than ~1 µm, at which a repulsive force was detected. This repulsion at the distances shorter than ~1 µm was not electrostatic in origin, but probably originated from both steric stabilization forces and viscoelastic forces; the former are caused by the compression of a hydrated layer of long-chain polymer molecules (proteins and carbohydrates) on the cell surface, while the latter result from the viscoelastic property of a cell [17]. During the dwell time of 5 min, no significant change was observed in the force–displacement curve and the microsphere was not likely to enter the B16F10 cell. Similar results were obtained for the untreated cells. Thus, the B16F10 cells never took up the 6.90-µm PS-COOH microspheres during the time period of 5 min.

13

It is still challenging to interpret the decompression force curve between the cell and material surfaces from a molecular point of view, because a large number of known/unknown adhesion processes can occur simultaneously [18] and the apical surface of cells often exhibits a rather rough and complex structure as shown in Fig. 2. For this reason, the magnitude of the attractive force at the initial de-adhesion peak (F_{adh}) will be used as a measure of the overall cell–microsphere adhesion force in Section 3.5.

3.5. Adhesion of a microsphere onto nanoparticle-treated cells

Figure 4b displays the distributions of adhesion force F_{adh} between the PS-COOH microsphere and the untreated cell ($t_{exp} = 0$) or the cell treated by 40-nm PS-COOH particles at $C_p = 0.08\%$ v/v for $t_{exp} =$ 15, 30, and 60 min. It is noted that F_{adh} is the force required for detaching the microsphere from the cell; the larger value of F_{adh} would indicate the stronger adhesion [18,19]. In the case of the untreated cells, the distribution of F_{adh} was rather broad and scattered, as seen from the interquartile range and the whisker range. Once the cells were treated by the nanoparticles, F_{adh} drastically diminished; indeed, the medians of F_{adh} for the treated cells ($t_{exp} = 15$, 30, and 60 min) were about one third of that for the untreated cells ($t_{exp} = 0$) and the distribution widths were remarkably reduced. The distribution width for F_{adh} seen from the interquartile range as well as the whisker range can be thought to depict the variation in the surface properties of individual cells, that is, the cell-to-cell difference in the number of sites on the individual cell surface that can bind with the microsphere surface. In this sense, the results of Fig. 4b indicate that the number of cellular binding sites available to the PS-COOH microsphere surface varied considerably from cell to cell in the case of the untreated cells, whereas its mean value as well as its variation was drastically diminished after 15-min exposure to the PS-COOH nanoparticles.

The malignant melanoma cells, such as B16F10 cell used in the present study, remarkably express several types of adhesion receptors from the integrin family of heterodimers of α and β subunits [20]. Our previous study [11] indicates that the COOH groups on the surface of PS-COOH microsphere

14

interacted somehow or other with the surface of B16F10 cell via integrins and the nonspecific COOH–integrin interaction was reduced by the presence of free Arg-Gly-Asp (RGD) peptides. Likewise, the 40-nm PS-COOH particles residing at the cell surface shown in Figs. 1b and 2 would interact with the cell surface by way of the nonspecific COOH–integrin interaction. It is most likely that the PS-COOH nanoparticles worked as a nonspecific competitive inhibitor of the adhesion of cell surface to the PS-COOH microsphere. This could explain why the adhesion force between the PS-COOH microsphere and cell surfaces was significantly reduced by exposure of the cells to the PS-COOH nanoparitcles (see Fig. 4b). It should be noted that the treatment by the nanoparticles hardly affected the morphology, the membrane integrity, and the metabolic activity of the B16F10 cells, as mentioned in Sections 3.2 and 3.3. Nevertheless, the nanoparticles could disturb the apical plasma membrane of the cells and some of its functions as observed in the earlier study [21], leading to the reduction of the microsphere–cell adhesion. In this sense, our AFM measurement of the microsphere–cell interactions successfully revealed the influence of the nanoparticles on the cells, which was never accessed by the other methods used in the present study (CLSM, SEM, and three different assays).

4. Conclusions

In summary, the adhesion force of single B16F10 cells to the surface of a 6.90-µm PS-COOH microsphere was significantly reduced by exposing them to the 40-nm PS-COOH nanoparticles in a serum-free culture medium, although the nanoparticle treatment of the cells hardly affected their morphology, membrane integrity, and metabolic activity. This is mainly because the PS-COOH nanoparticles worked as a nonspecific competitive inhibitor of the adhesion of cell surface to the PS-COOH microsphere, and partly because the nanoparticles could disturb somehow or other the apical plasma membrane of the cells and some of its functions. In this sense, our AFM measurement of the

microsphere–cell interactions successfully revealed the influence of the nanoparticles on the cells, which was never accessed by the other methods used in the present study (CLSM, SEM, and three different assays).

Fig. 1. Confocal laser scanning micrographs of B16F10 cells after 40-nm PS-COOH particle exposure of period t_{exp} = 180 min and concentration C_p = 0.08% v/v: (a) Differential interference contrast image and (b) fluorescence image of the optical section near the glass-bottom surface. Scale bars: 50 μm. (c) Fluorescence per cell as a function of t_{exp} for C_p = 0.08% v/v. The line shows the fitting curve given by Eq. (5).

Fig. 2. (a) Scanning electron micrograph of B16F10 cells after 40-nm PS-COOH particle exposure of period t_{exp} = 15 min and concentration C_p = 0.08% v/v and (b) the magnification of its central region.

Fig. 3. The short-term responses of B16F10 cells to 40-nm PS-COOH particles as function of nanoparticle concentration C_p for different exposure periods of t_{exp} = 30 and 180 min: (a) trypan blue assay, (b) LDH assay, and (c) ATP assay. No significant difference was observed between the treated groups (C_p > 0) and the control group (C_p = 0).

Fig. 4. (a) Force–displacement curves during compression (upper, red colored) and decompression (lower, blue colored) measured between a 6.90-μm PS-COOH microsphere and a treated B16F10 cell (t_{exp} = 60 min) in nanoparticle-free DMEM. (b) The box plots of the distributions of adhesion force F_{adh} between the PS-COOH microsphere and the untreated cell (t_{exp} = 0) or the cell treated by 40-nm PS-COOH particles at C_p = 0.08% v/v for t_{exp} = 15, 30, and 60 min. Each box plot shows six-number summaries: the 0.05-fractile, first quartile, median, third quartile, and 0.95-fractile as well as the mean (solid square plot). Significant differences of $P \leq 0.05$ and $P \leq 0.01$ for the treated groups versus the control group (t_{exp} = 0) are depicted by the asterisk (*) and the double asterisks (**), respectively.

Table 1

The results of characterization of PS-COOH nanoparticles and PS-COOH microspheres suspended in water or DMEM at 25.0 °C

dispersoid	medium	Z-average size	PDI[a]	Zeta potential (mV)
nanoparticles	water	40.0 nm	0.12	−34
	DMEM	38.4 nm	0.11	−11
microspheres	water	$6.90 \pm 0.41 \ \mu m$[b]		−52
	DMEM			−15

[a] Polydispersity index

[b] The volume mean average diameter with the standard deviation is given according to the manufacturer's data sheet.

References

[1] V. Mailänder, K. Landfester, Biomacromolecules, 10 (2009) 2379-2400.

[2] F. Zhao, Y. Zhao, Y. Liu, X. Chang, C. Chen, Y. Zhao, Small, 7 (2011) 1322-1337.

[3] A. Nel, T. Xia, L. Madler, N. Li, Science, 311 (2006) 622-627.

[4] G. Oberdörster, E. Oberdörster, J. Oberdörster, Environ. Health Perspect., 113 (2005) 823-839.

[5] A. Dhawan, V. Sharma, Analytical Bioanalytical Chemistry, 398 (2010) 589-605.

[6] A.E. Nel, L. Madler, D. Velegol, T. Xia, E.M.V. Hoek, P. Somasundaran, F. Klaessig, V. Castranova, M. Thompson, Nature Materials, 8 (2009) 543-557.

[7] R.N. Grass, L.K. Limbach, E.K. Athanassiou, W.J. Stark, Journal of Aerosol Science, 41 (2010) 1123-1142.

[8] A. Petushkov, N. Ndiege, A.K. Salem, S.C. Larsen, in: C.F. James (Ed.) Advances in Molecular Toxicology, Vol. 4, Elsevier, 2010, Chapter 7.

[9] W. Wallace, M. Keane, D. Murray, W. Chisholm, A. Maynard, T.-m. Ong, Journal of Nanoparticle Research, 9 (2007) 23-38.

[10] H. Hillaireau, P. Couvreur, Cellular and Molecular Life Sciences, 66 (2009) 2873-2896.

[11] H. Shinto, Y. Aso, T. Fukasawa, K. Higashitani, Colloids Surf. B: Biointerfaces, 91 (2012) 114-121.

[12] M. Benoit, H.E. Gaub, Cells Tissues Organs, 172 (2002) 174-189.

[13] J. Rejman, V. Oberle, I.S. Zuhorn, D. Hoekstra, Biochem. J., 377 (2004) 159-169.

[14] D. Guarnieri, A. Guaccio, S. Fusco, P.A. Netti, Journal of Nanoparticle Research, 13 (2011) 4295-4309.

[15] T. Xia, L. Rome, A. Nel, Nature Materials, 7 (2008) 519-520.

[16] A. Verma, O. Uzun, Y. Hu, Y. Hu, H.-S. Han, N. Watson, S. Chen, D.J. Irvine, F. Stellacci, Nature Materials, 7 (2008) 588-595.

[17] S. Iyer, R.M. Gaikwad, V. Subba-Rao, C.D. Woodworth, I. Sokolov, Nat. Nanotechnol., 4 (2009) 389-393.

[18] J. Helenius, C.-P. Heisenberg, H.E. Gaub, D.J. Müller, J. Cell. Sci., 121 (2008) 1785-1791.

[19] A. Taubenberger, D.A. Cisneros, J. Friedrichs, P.-H. Puech, D.J. Müller, C.M. Franz, Mol. Biol. Cell, 18 (2007) 1634-1644.

[20] R.H. Kramer, M. Vu, Y.-F. Cheng, D.M. Ramos, Cancer Metastasis Rev., 10 (1991) 49-59.

[21] C. Brandenberger, B. Rothen-Rutishauser, F. Blank, P. Gehr, C. Muhlfeld, Respir. Res., 10 (2009) 22.
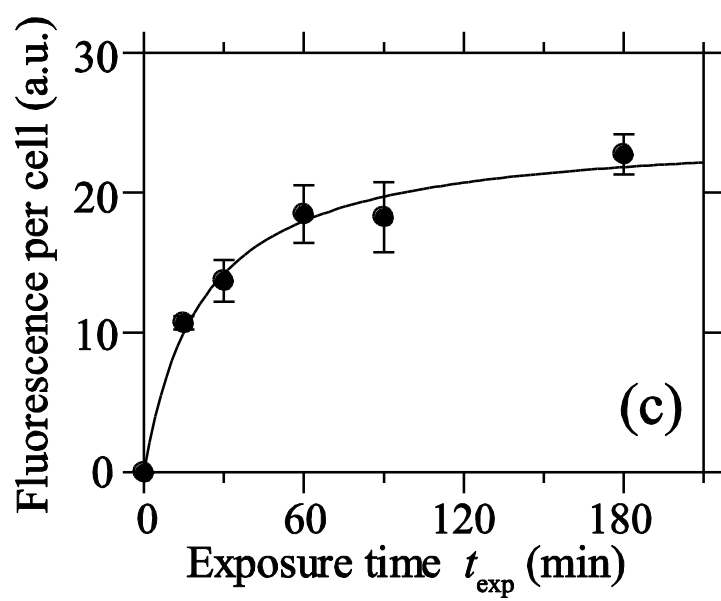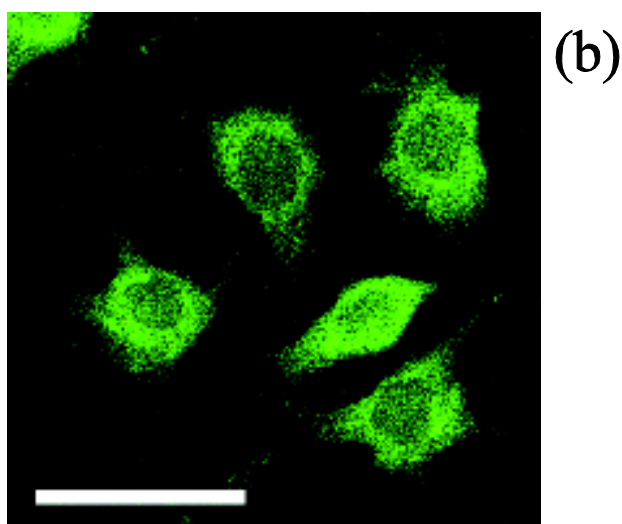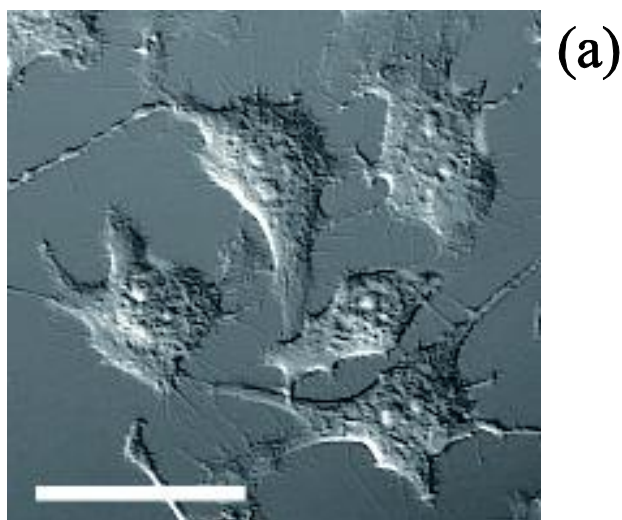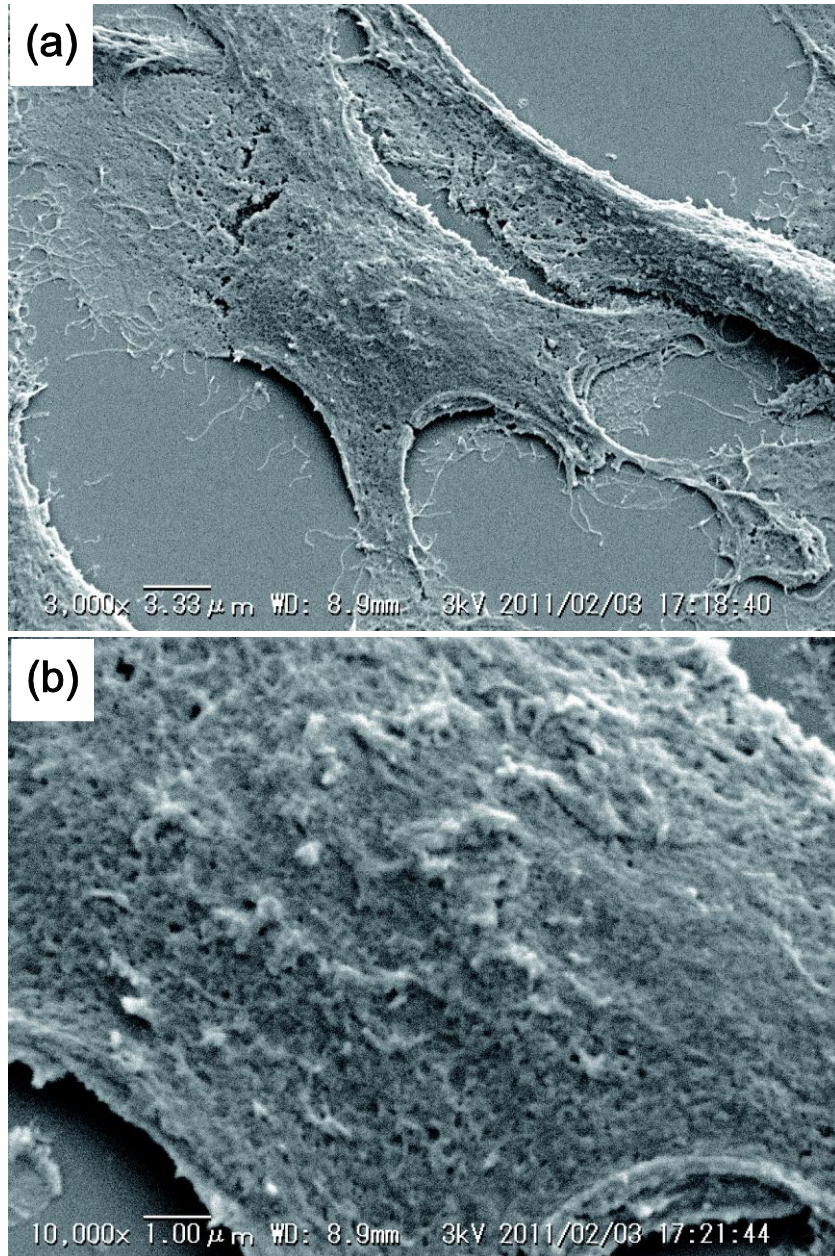
Fig. 1

(a)

(b)

(c)

Fig. 2

(a)

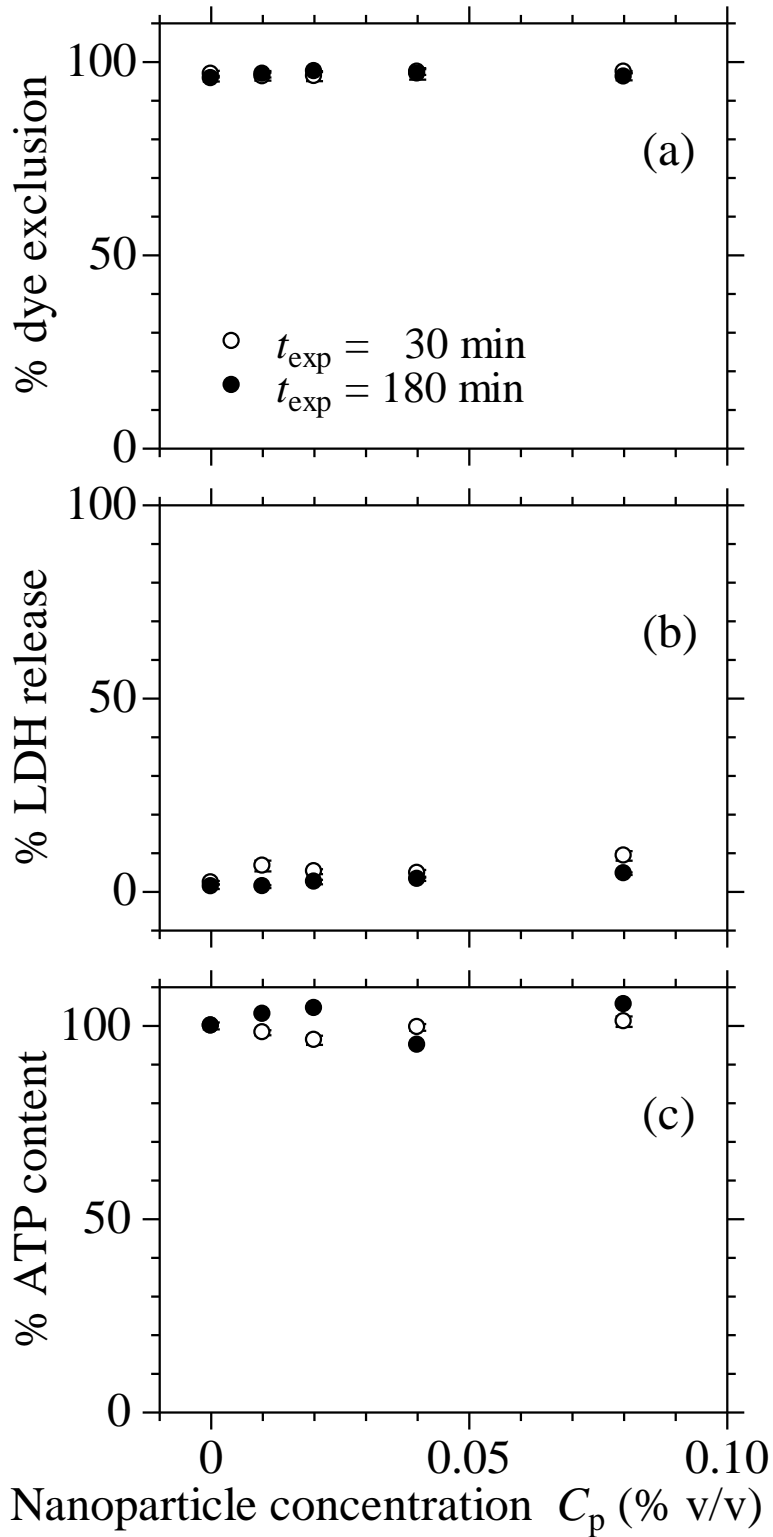3,000× 3.33 μm WD: 8.9mm 3kV 2011/02/03 17:18:40

(b)

10,000× 1.00 μm WD: 8.9mm 3kV 2011/02/03 17:21:44

Fig. 3 Shinto et al.

Fig. 4